**Review article**

Kazuhide Nakajima*, Kotaro Saito, Yusuke Yamada, Kenji Kurokawa, Tomoya Shimizu, Chisato Fukai and Takashi Matsui

# Holey fibers for low bend loss

**Abstract:** Bending-loss insensitive fiber (BIF) has proved an essential medium for constructing the current fiber to the home (FTTH) network. By contrast, the progress that has been made on holey fiber (HF) technologies provides us with novel possibilities including non-telecom applications. In this paper, we review recent progress on hole-assisted type BIF. A simple design consideration is overviewed. We then describe some of the properties of HAF including its mechanical reliability. Finally, we introduce some applications of HAF including to high power transmission. We show that HAF with a low bending loss has the potential for use in various future optical technologies as well as in the optical communication network.

**Keywords:** hole assisted fiber; bending loss; fiber to the home; splicing technique; mechanical reliability; fiber fuse.

***Corresponding author: Kazuhide Nakajima,** Access Network Service Systems Laboratories, NTT Corporation, 1-7-1, Hanabatake, Tsukuba, Ibaraki, 305-0805, Japan, e-mail: nakajima.kazuhide@lab.ntt.co.jp

**Kotaro Saito, Yusuke Yamada, Tomoya Shimizu, Chisato Fukai and Takashi Matsui:** Access Network Service Systems Laboratories, NTT Corporation, 1-7-1, Hanabatake, Tsukuba, Ibaraki, 305-0805, Japan

**Kenji Kurokawa:** Department of Electrical and Electronic Engineering, Kitami Institute of Technology, 165, Koen-cho, Kitami, Hokkaido, 090-8507, Japan

**Edited by David J. DiGiovanni**

## 1 Introduction

Fiber to the home (FTTH) has been widely deployed because of the growing demand for broadband services. And bending-loss insensitive fiber (BIF) has become a key technology in recent access networks. This is because a large bending loss in conventional single-mode fiber (SMF) [1] can restrict its ease of handling and/or its applicable area. Thus, various kinds of BIF have been developed [2–5] to realize FTTH networks that are easy and economical to install and maintain. BIF has been standardized in the Telecommunication Standardization Sector of the International Telecommunication Union (ITU-T) as Recommendation G.657 [6], and the latest version considers a minimum bending radius of 5 mm.

Novel research on holey fibers (HFs) was undertaken in the 1970s–1980s. Kaiser reported a single-material fiber with an air cladding [7]. Okoshi proposed a side-tunnel fiber to obtain a polarization maintaining waveguide [8]. Research on HFs accelerated particularly after Birks reported on bandgap characteristics using a two-dimensional periodic air hole structure [9]. HF enables us to realize novel transmission characteristics that cannot be obtained with a conventional SMF. The endlessly single-mode (ESM) characteristic can be considered one of the most important properties of a photonic crystal fiber (PCF) [10, 11]. This is because an ESM-PCF with low loss directly opens up a novel single-mode transmission window. Tajima achieved the lowest loss of 0.18 dB/km [12]. With this as the background, various transmission experiments have been conducted to confirm the validity of ESM-PCF as an ultra wideband transmission medium [13–17]. The unique characteristics of HFs mainly derive from the large refractive index difference between silica glass and an air hole. This feature can be obtained simply by introducing several air holes into conventional SMF. Hole assisted fiber (HAF) enables us to realize unique dispersion characteristics [18]. The use of several air holes can greatly improve the bending loss insensitivity [19]. Recent reports have also pointed out the applicability of a hole assisted structure as a high power light guide [20, 21].

In this paper, we review recent progress on HAF based BIF technologies. In section 2, we briefly explain the design considerations as regards HAF by using a rough approximation model. Section 3 describes the properties of fabricated HAF. Here, we consider not only the transmission characteristics but also the mechanical reliability of the hole-assisted structure. In section 4, we describe a technique for splicing HAF taking various existing techniques into account. In section 5, we introduce some applications of HAF including its applicability to high power transmission. Finally, we conclude our review article with a brief summary.

## 2 Design of HAF

Figure 1 shows a schematic cross sectional image of a HAF. HAF has a conventional doped core with a diameter 2a. We defined a relative index difference of the core as Δ. Basically, the core and cladding constitute a lightguide. *N* air holes with a diameter *d* are arranged in a circle around the core. In Figure 1 *N*=10 is shown as an example, and we assume $R_{In}$ and $R_{Out}$ to be inscribed and circumscribed radii, respectively. Here, an equivalent refractive index profile of HAF can be assumed with a trench structure [2], where the air hole region constitutes the low index ring as shown on right hand side of Figure 1.

The properties of HF (i.e., a fiber with an arbitrary two-dimensional structure) can be calculated by using the finite element method (FEM) [22, 23]. The characteristics of HAF can be easily estimated by considering the influence of the air holes on the electric field of the base lightguide. In general terms, the electric field is greatly affected when $R_{In}$ and/or the equivalent refractive index of the air hole region become small. Figure 2 shows the relative difference in the mode-field diameter (MFD) at 1550 nm as a function of the normalized inscribed circle radius $R_{In}$/a. The two solid lines show the calculated results. The blue line corresponds to a conventional SMF (i.e., without air holes). The open circles show measured results obtained for two HAFs. Here, *N* and *d* were 10 and 0.4 times 2a, respectively. It can be seen from Figure 2 that the MFD becomes small as $R_{In}$/a decreases. These results show that the confinement property of the original electric field can be managed by controlling the air hole arrangement.

We then introduced an air filling fraction *S* as Eq. (1) [24] to make it easy to understand the relationship between the air hole design condition and the transmission properties.

$$S \equiv \frac{N(d/2)^2}{R_{Out}^2 - R_{In}^2} \tag{1}$$

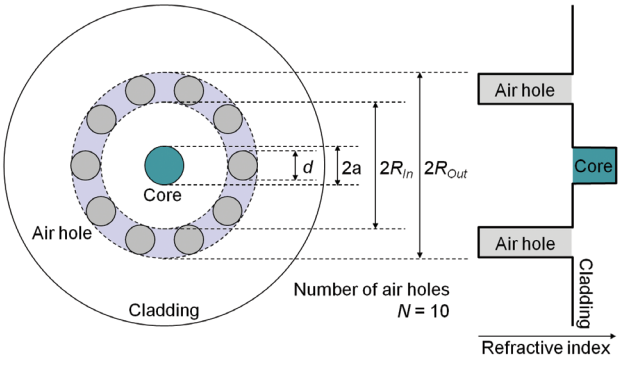


**Figure 1** Cross sectional image of HAF.

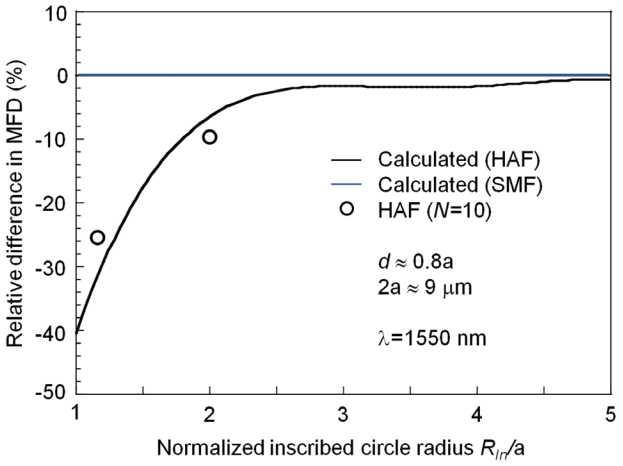


**Figure 2** Influence of inscribed circle radius $R_{In}$ on MFD.

Figure 3 shows the *S*-value dependence of HAF. (A) and (B) show the bending loss $\alpha_b$ and cut-off wavelength $\lambda_{cc}$ characteristics, respectively. $\alpha_b$ was evaluated at 1625 nm with a 5 mm bending radius. The filled symbol indicates the result for SMF. The open circles and squares

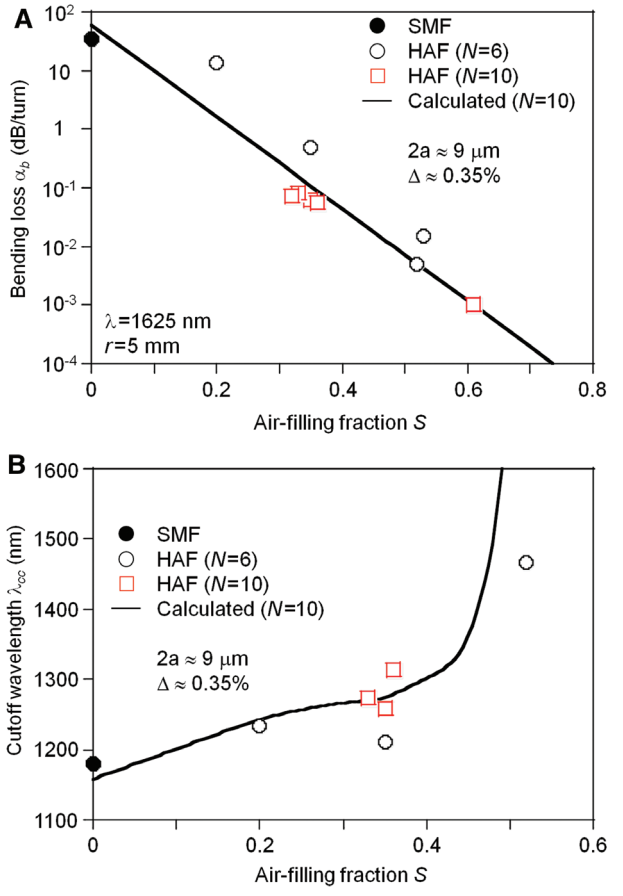


**Figure 3** Air filling fraction *S* dependence of (A) bending loss $\alpha_b$ and (B) cut-off wavelength $\lambda_{cc}$.

correspond to HAF with $N$=6 and 10, respectively. Here, the $R_{In}$/a values were in the 1.2 to 3.5 range. The 2a and Δ values of all the fibers, including SMF, were about 9 μm and 0.35%, respectively. The solid lines show the calculated results when $R_{In}$/a=2 and $N$=10. It is difficult to determine the $\lambda_{cc}$ of HAF by considering the cladding index since the effective index value becomes lower than the silica level depending on the air holes. We then determined the $\lambda_{cc}$ of HAF as the wavelength at which the confinement loss of the first higher order mode reaches 1 dB/m [25]. Figure 3 confirms that the measured and calculated results reveal a similar tendency. With respect to the $\alpha_b$ characteristic, Figure 3A shows that $\alpha_b$ decreases exponentially as the $S$ value increases. Figure 3B also shows that $\lambda_{cc}$ becomes longer as the $S$ value increases. However, it should be noted that the $\lambda_{cc}$ of HAF is greatly affected particularly when $S$ exceeds 0.45. This is because the region surrounded with air holes supports another guided mode independent of the existence of a doped core.

Figure 4A and B show the Δ-value dependence of $\alpha_b$ and $\lambda_{cc}$, respectively. The open squares show the measured results for HAFs with $N$=10. All HAFs had a similar $S$-value of about 0.35. The solid lines show the calculated results for SMF (i.e., without air holes). In Figure 4A, the dashed line shows the calculted results for HAF ($N$=10) for comparison, and it is almost parallel to the solid line. Thus, Figure 4A and B show that the Δ dependence of $\alpha_b$ and $\lambda_{cc}$ can be considered similar to that in a conventional SMF.

These results reveal that the $\alpha_b$ and $\lambda_{cc}$ characteristics of HAF can be approximated by considering the $S$- and Δ-value dependence. As a result, we can derive the following two empirical relations [24].

$$\ln(\alpha_b) \approx \ln(b_1) + b_2 \cdot S + b_3 \cdot \delta\Delta \quad (2)$$

$$\lambda_c \approx c_1 + c_2 \cdot S + c_3 \cdot \delta\Delta \quad (3)$$

Here, $b_i$ and $c_i$ ($i$=1, 2, and 3) denote coefficients, and $\delta\Delta$ shows the relative difference in an arbtirary reference Δ value. These emprical relationships are sufficiently useful for roughly designing a HAF with the desired characteristics since we can easily utilize the well known design used for conventional SMF as a basis.

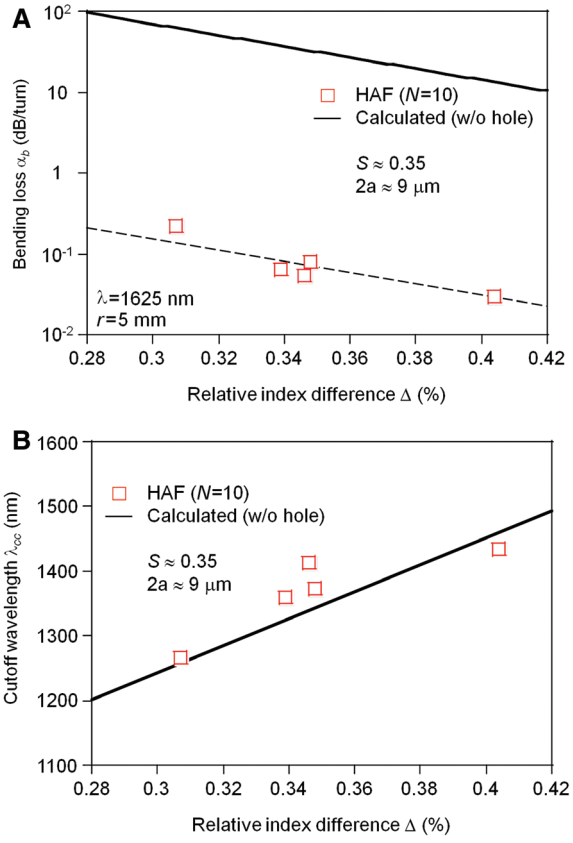


**Figure 4** Δ Dependence of (A) bending loss $\alpha_b$ and (B) cut-off wavelength $\lambda_{cc}$.

# 3 Properties of HAF

In this section, we introduce example properties of HAF. The transmission properties of fabricated HAFs are described including the impact of bending loss Insensitivity on the transmission performance. We also investigate the mechanical reliability of a hole assisted structure.

## 3.1 Characteristics of fabricated HAFs

Table 1 summarizes example characteristics of HAFs. We fabricated two HAFs. Each HAF had different air hole design conditions in terms of their $S$, $R_{In}$, and $N$ values,

**Table 1** Characteristics of fabricated HAFs.

| | HAF1 | HAF2 |
|---|---|---|
| Core diameter 2a (μm) | 7.8 | 7.8 |
| Relative index difference Δ (%) | 0.31 | 0.31 |
| Air-filling fraction $S$ | 0.49 | 0.41 |
| Normalized inscribed circle radius $R_{In}$/a | 2.1 | 2.8 |
| Number of air holes $N$ | 6 | 10 |
| MFD 2$W$ at1310 nm (μm) | 8.9 | 9.0 |
| Cutoff wavelength $\lambda_{cc}$ | 1118 | 1126 |
| Bending loss $\alpha_b$ at 1625 nm, $r$=5mm (dB/turn) | 0.05 | 0.04 |
| Zero-dispersion wavelength $\lambda_0$ (nm) | 1318 | 1321 |
| Zero-dispersion slope $s_0$ (ps/nm²·km) | 0.098 | 0.090 |

 

although both HAFs had a similar core structure of 2a=7.8 μm and Δ=0.31%. The MFD values of the two HAFs were comparable. The $\lambda_{cc}$ values measured with a 22 m long sample were <1260 nm. These MFD and $\lambda_{cc}$ values meet the specifications of conventional SMF [1]. The $\alpha_b$ values of the two HAFs were <0.1 dB/turn at 1625 nm with a 5 mm bending radius.

Table 2 summarizes the BIF categories used in ITU-T Recommendation G.657 [6]. BIF is categorized into four types (A1, A2, B2, and B3) considering two viewpoints. The first viewpoint takes bending loss insensitivity into consideration. The allowable minimum bending radius $R_{min}$ of conventional SMF is limited to 30 mm, but BIF has three levels. Levels 1, 2 and 3 set the $R_{min}$ values at 10, 7.5, and 5 mm, respectively. The $\alpha_b$ specification for level 3 is <0.45 dB/turn at 1625 nm with $R_{min}$=5 mm. Thus, it can be confirmed that the two fabricated HAFs summarized in Table 1 satisfy the highest requirement for bending loss insensitivity.

The second viewpoint considers compliance with conventional SMF [1]. Class A is fully compliant with conventional SMF, but class B is not. Here, compliant means that there is no difference in the dispersion properties. In this case, the zero-dispersion wavelength $\lambda_0$ and maximum zero-dispersion slope $s_0$ of conventional SMF are specified at 1300–1324 nm and 0.092 ps/nm²·km or less, respectively. Figure 5 shows the calculated $R_{In}$/a dependence of $\lambda_0$ and $s_0$ in HAF with $N$=10. The 2a, Δ and $S$ values were set at 9 μm, 0.3%, and 0.4, respectively. Table 1 and Figure 5 confirm that the dispersion properties of HAF can also be tailored by controlling the $R_{In}$/a value. Therefore, these results reveal that a BIF with the desired transmission properties can be realized easily by appropriately designing the hole assisted structure.

**Table 2** Classification of BIF in ITU-T recommendation G.657 [6].

| | Bending loss property | | |
|---|---|---|---|
| | **Level 1** | **Level 2** | **Level 3** |
| **Class A** Fully compliant (*) with standard SMF | A1 | A2 | No specification |
| **Class B** Not fully compliant with standard SMF | No specification | B2 | B3 |

(*) Compliant means that there is no difference in dispersion properties (zero-dispersion wavelength $\lambda_0$ and zero-dispersion wavelength slope $s_0$)

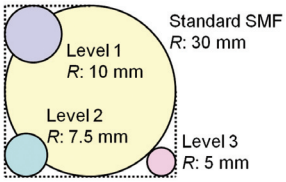


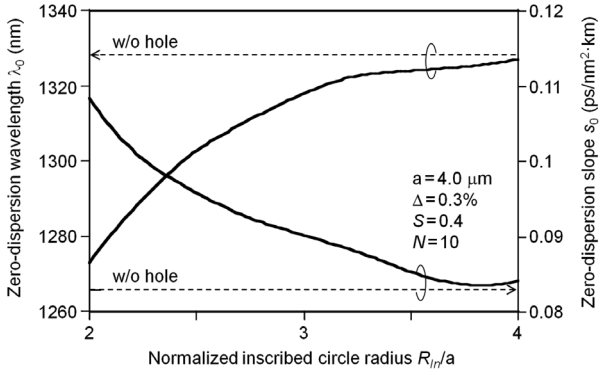


**Figure 5** Zero-dispersion wavelength $\lambda_0$ and zero-dispersion slope $s_0$ of HAF as a function of normalized inscribed circle radius $R_{In}$/a.

We then investigated the impact of bending loss insensitivity on transmission performance. Here, we considered the multi-path interference (MPI) characteristic. MPI is an interference noise between two signals with different optical paths, and can be measured using the simple experimental set up shown in Figure 6 [25]. Moreover, MPI is known to be related to transmission performance [26]. Recently, ITU-T studied an MPI measurement technique in relation to the single-mode operability of BIF [27] since the bending loss insensitivity also affects the higher order mode.

We evaluated the MPI characteristics of the HAFs shown in Table 1. By using the experimental set up shown in Figure 6, MPI can be measured by observing the optical received power with a sufficient number of wavelengths and polarization states. Figure 7 shows the relative degradation in MPI as a function of bending radius. The measurement wavelength was 1550 nm. The number of turns was fixed at 10 for each bending radius. The filled and open symbols show the results obtained with conventional SMF and HAFs, respectively. Figure 7 shows that the MPI in SMF clearly degraded as the bending radius decreased. This is because the leaked light induced by a small bend interferes with the guided light. By contrast, the MPI values in the HAFs were almost insensitive to the bending radius. These results confirm that a BIF with

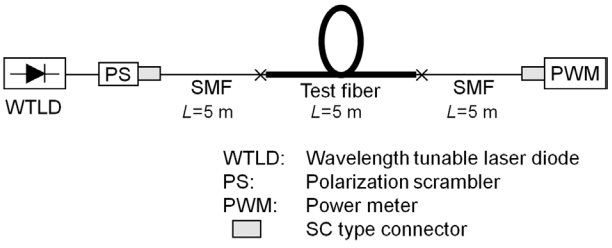


**Figure 6** Experimental set up for measuring multi-path interference (MPI).

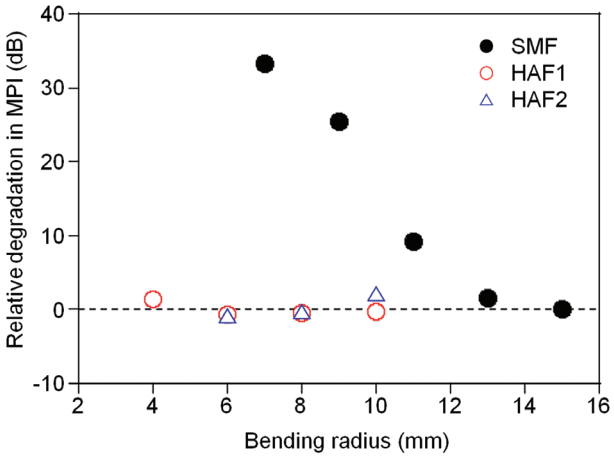


**Figure 7** Relative degradation in multi-path interference (MPI) as a function of bending radius.

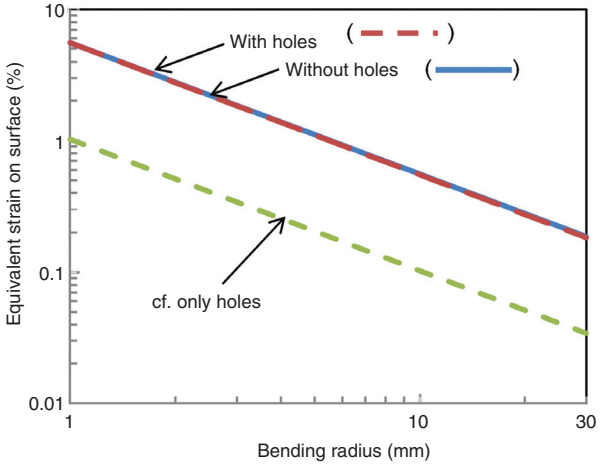


**Figure 9** Relationship between radius and calculated equivalent strain.

sufficient bending loss insensitivity has a great impact on transmission performance in terms of MPI degradation.

## 3.2 Mechanical reliability

BIFs as HAFs can be bent with a smaller diameter than conventional fiber because of their low bending loss characteristics. However, it is well-known that the mechanical reliability of optical fiber deteriorates when it is under excessive stress induced by bending. Therefore, when we wish to apply HAFs to telecommunication systems, it is important that we clarify their mechanical reliability. Here we describe the effect of the holes on the fatigue characteristics.

### 3.2.1 Strain of bent HAF

Figure 8 shows the geometry of a bent HAF. The dominant factor in the fracture is the tensile strain applied to the surface. Therefore, to estimate the fatigue characteristics of HAF, it is necessary to consider not only the strain of the cladding surface but also the inner surface of the holes.

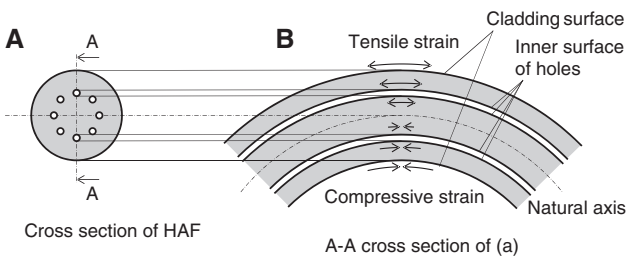


**Figure 8** Geometry of bent HAF.

Figure 9 shows the relationship between bending radius and calculated equivalent strain. Here, the equivalent strain is calculated by integrating the strain of the surface [28]. The blue and red lines show the conventional fiber (without holes) and HAF (with holes). The green dashed line show the result when we calculated equivalent strain on the only inner surfaces of the holes. As a result, the equivalent strain on the inner surfaces of the holes is small compared with that of the cladding surface. Also, the equivalent strain of the HAF and conventional fiber are almost the same. This is because the strain and the area to which it is applied on the inner surface of the hole are smaller than that of the cladding surface. In addition, we calculated the strain induced by bending.

Figure 10 is an example of calculated results by the FEM. We found that the strain intensified at the cladding surface and the holes did not affect the stress distribution in the cross section.

### 3.2.2 Characterization of mechanical reliability

There are several techniques for mechanically testing optical fiber. We have proposed a slotted bending fixture

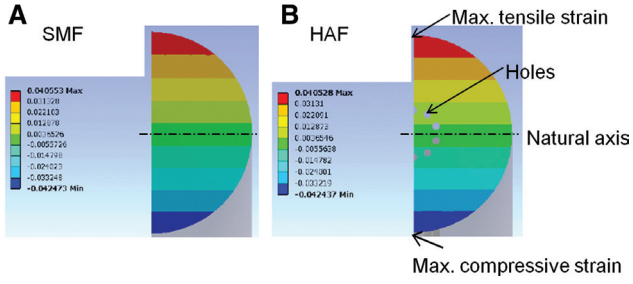


**Figure 10** Stress distribution in cross section.

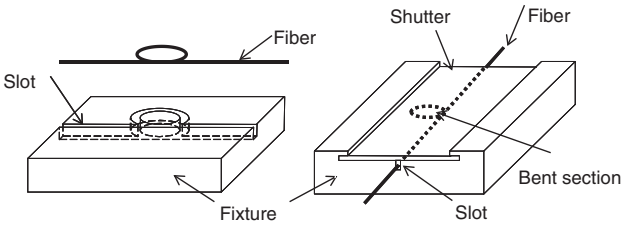


**Figure 11** Schematic diagram of slotted bend fixture.

for realizing uniform and tight bending conditions [29]. Figure 11 is a schematic of the slotted bending fixture used in our experiments. It is composed of a slotted plate and a shutter, and it can induce a uniform bending strain in a test fiber. By constructing several fixtures with different slot radii, we could vary the uniformly applied bending strain systematically.

We performed static fatigue tests on two kinds of HAFs and conventional fiber. Figure 12 shows the static fatigue characteristics of the fibers. Here, time to failure is measured the fracture time of 30–40 specimens at each of bending diameters each types of fibers. The solid lines are the power approximation curves to the median values. We found that the times to failure of HAFs and conventional SMFs differed slightly. As shown Figure 12, the measured time to failure of HAFs was 50% longer than that of conventional SMF. The reason for this might be the relaxation of crack growth and/or cladding surface stress caused by the holes. However, the reason for the difference in the time to failure of HAFs has not yet been completely explained. We need further study on the mechanical reliability of hole assisted structure including its dependence on sir hole arrangement.

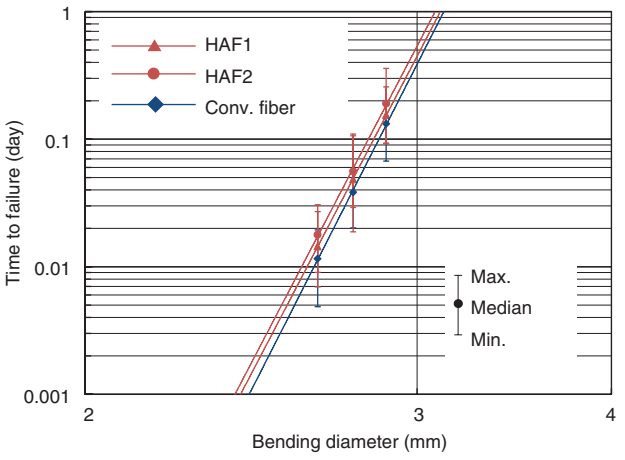


**Figure 12** Static fatigue characteristics under smaller-bending condition.

# 4 Splicing techniques

Various splicing techniques, including fusion, connector, and mechanical splicing, are used in optical networks. When we apply HAF to an optical network, it is important to clarify its splicing characteristics.

## 4.1 Fusion splicing

First we examined fusion splicing characteristics. In fusion splicing, an arc discharge collapses the air holes, thus the MFD difference between the hole region and the collapsed hole region at a fusion splice point can cause MFD mismatch loss [30]. To suppress the MFD mismatch loss, we used HAF whose MFD was appropriately designed in terms of $V$, $S$, and $R_{In}$/a and also used the sweep discharge method [30]. Here, $V$ corresponds to the normalized frequency of conventional SMF, and it can be derived by using the 2a and $\Delta$ values of the core. Table 3 summarizes the fusion splice loss characteristics. Table 3 shows that the average splice losses for HAF -HAF were 0.04 dB at 1310 nm and 0.07 dB at 1550 nm. It also shows that the average splice losses for SMF-HAF were 0.06 dB at 1310 nm and 0.07 dB at 1550 nm. These results confirm that the HAF can be fusion spliced with a sufficiently low splice loss independent of the existence of air holes.

Figure 13A and B show the results of a temperature cycle test at 1310 and 1550 nm based on Telcordia GR-326. Figure 13 confirms that the fluctuation in the fusion splice losses was <0.01 dB at both 1310 and 1550 nm. Therefore, satisfactory fusion splice characteristics can be obtained for HAF including the temperature cycle characteristics.

## 4.2 Connectorized optical cord

Second, we investigated the characteristics of HAF based optical cord with a conventional SC type connector.

**Table 3** Fusion splice loss characteristics.

| | SMF-HAF | HAF-HAF |
|---|---|---|
| 1310 nm | | |
| Average | 0.06 | 0.04 |
| Maximum | 0.10 | 0.07 |
| Minimum | 0.03 | 0.02 |
| 1550 nm | | |
| Average | 0.07 | 0.07 |
| Maximum | 0.10 | 0.09 |
| Minimum | 0.05 | 0.06 |

Sample number: 20.

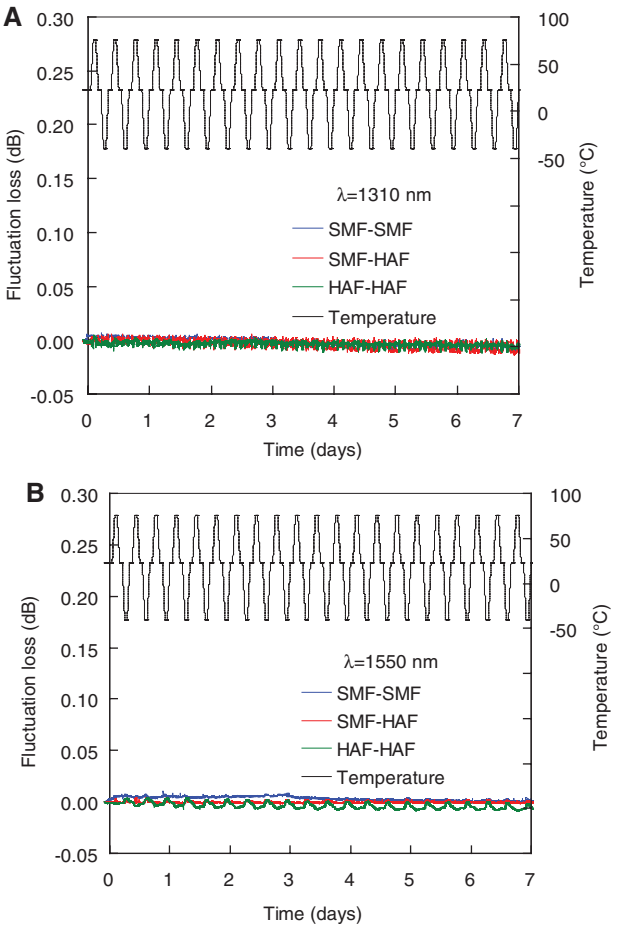


**Figure 13** Temperature cycle test results at (A) 1310 nm and (B) 1550 nm.

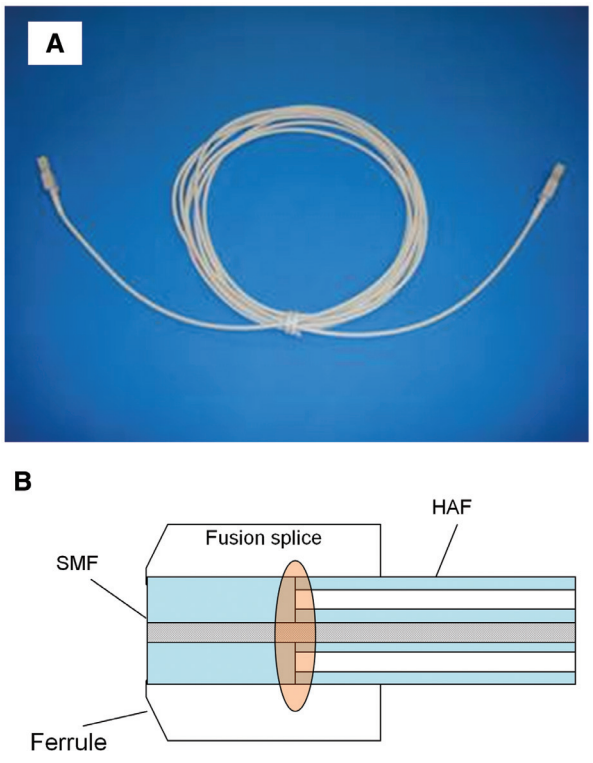


**Figure 14** (A) Photograph of HAF cord with SC connectors, (B) Schematic image of mechanical splice point.

## 4.3 Mechanical splicing

Figure 14 shows (A) a photograph of a HAF cord and (B) an image of a ferrule portion. The HAF cord was 5 m long. The HAF endface should generally be sealed when a conventional connector is used. This is because unexpected contamination of the air hole region may degrade the splice characteristics. Thus, we fusion spliced the HAF with conventional SMF in the attached SC connector, and adequately polished the other end of the SMF. We then examined the splice characteristics of the fabricated HAF cord. Table 4 summarizes the insertion and return losses measured with ten HAF cords. Average insertion losses of 0.33 dB at 1310 nm and 0.36 dB at 1550 nm were obtained. The average return losses were 48.3 dB at 1310 nm and 51.6 dB at 1550 nm. Figure 15 shows the results of a temperature cycle test. The insertion loss fluctuation of the HAF cord was <0.1 dB at both 1310 and 1550 nm. As a result, we confirmed that we could obtain satisfactory splicing characteristics with HAF cord.

Third, we examined the characteristics of mechanical splicing. Normally mechanical splicing uses a liquid refractive index matching material to reduce the Fresnel reflection induced by the air gap between fiber endfaces. When we splice HAF with a conventional mechanical splice, the splice loss increases, because liquid refractive index matching material penetrates the air holes. Figure 16 shows a schematic image of a mechanical splice point. The refractive index of the matching material is greater than the refractive index of the cladding. So the refractive index matching material that penetrates the holes functions as

**Table 4** Insertion and return losses of HAF-based optical cord.

| | Insertion loss | Return loss |
|---|---|---|
| 1310 nm | | |
| Average | 0.33 | 48.3 |
| Maximum | 0.53 | 49.1 |
| Minimum | 0.16 | 45.8 |
| 1550 nm | | |
| Average | 0.36 | 51.6 |
| Maximum | 0.43 | 53.2 |
| Minimum | 0.27 | 49.6 |

Sample number: 10.

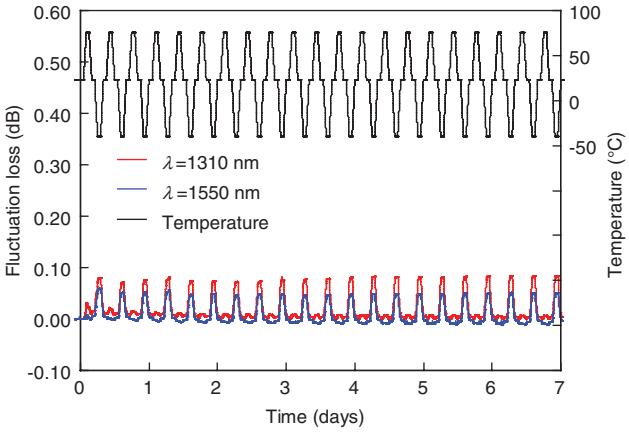


**Figure 15** Temperature cycle test on HAF-based optical cord.

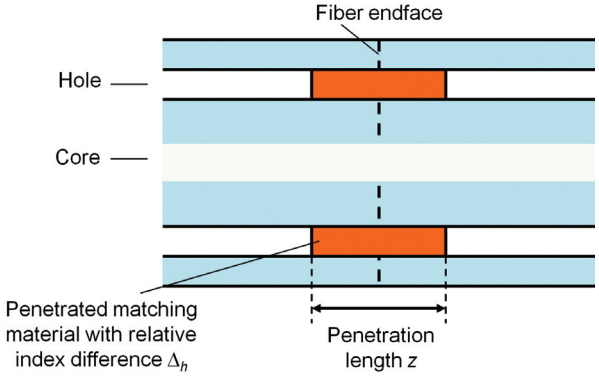


**Figure 16** Schematic image of mechanical splice point.

a core, forming an asymmetrical parallel waveguide. As a result, some of the light in the core is transferred to the refractive index matching material in the air holes. Therefore, we developed a solid type refractive index matching material and clarified the optimum mechanical splice conditions in terms of penetration length $z$, the relative index difference of the matching material $\Delta_h$, and the temperature dependence of the refractive index $dn/dT$ [31, 32].

Tables 5 and 6 summarize the splice and return loss characteristics obtained when using solid optimized refractive index matching material. Here, a thickness of our matching material was well controlled at <200 μm. It can be considered that $z$ value was also controlled to be <100 μm (a half of the thickness) since it has adequate hardness. Table 5 confirms that the average splice losses at (1310 nm, 1550 nm) of SMF-SMF, SMF-HAF, and HAF-HAF are (0.10 dB, 0.08 dB), (0.07 dB, 0.08 dB), and (0.06 dB, 0.08 dB), respectively. Table 6 also shows that the average return losses at (1310 nm, 1550 nm) of SMF-SMF, SMF-HAF, and HAF-HAF were (57.0 dB, 58.8 dB), (57.0 dB, 58.2 dB), and (58.2 dB, 59.2 dB), respectively. Figure 17 shows the

**Table 5** Mechanical splice loss characteristics.

| | SMF-SMF | SMF-HAF | HAF-HAF |
|---|---|---|---|
| 1310 nm | | | |
| Average | 0.10 | 0.07 | 0.06 |
| Maximum | 0.15 | 0.14 | 0.13 |
| Minimum | 0.04 | 0.03 | 0.00 |
| 1550 nm | | | |
| Average | 0.08 | 0.08 | 0.08 |
| Maximum | 0.15 | 0.14 | 0.14 |
| Minimum | 0.04 | 0.04 | 0.01 |

Sample number: 20.

**Table 6** Return loss characteristics of mechanical splice.

| | SMF-SMF | SMF-HAF | HAF-HAF |
|---|---|---|---|
| 1310 nm | | | |
| Average | 57.0 | 57.0 | 58.2 |
| Maximum | 65.0 | 62.0 | 62.7 |
| Minimum | 51.3 | 53.4 | 51.9 |
| 1550 nm | | | |
| Average | 58.8 | 58.2 | 59.2 |
| Maximum | 65.0 | 65.0 | 65.0 |
| Minimum | 51.3 | 52.6 | 53.9 |

Sample number: 20.

results of a temperature cycling test. The splice loss fluctuation of the mechanical splice was <0.05 dB at both 1310 and 1550 nm. As a result, we can splice HAF with satisfactory splice characteristics that are comparable to those of SMF splices characteristics including temperature cycle characteristics.

# 5 Application of HAF

In this section, we introduce some example applications of HAF. We also investigate its applicability as a high power transmission medium.

## 5.1 Application in optical access network

As mentioned in the introduction, bending loss insenitive HAF (BI-HAF) is expected to be a key medium for solving the construction and/or handling problems of the FTTH network. Figure 18 shows an example of BI-HAF applications in an optical access network. First, NTT utilizes a BI-HAF on the customer's premises. The optical wiring requirements of indoor optical cable differ depending on the premises. It may be difficult to obtain an optical wiring

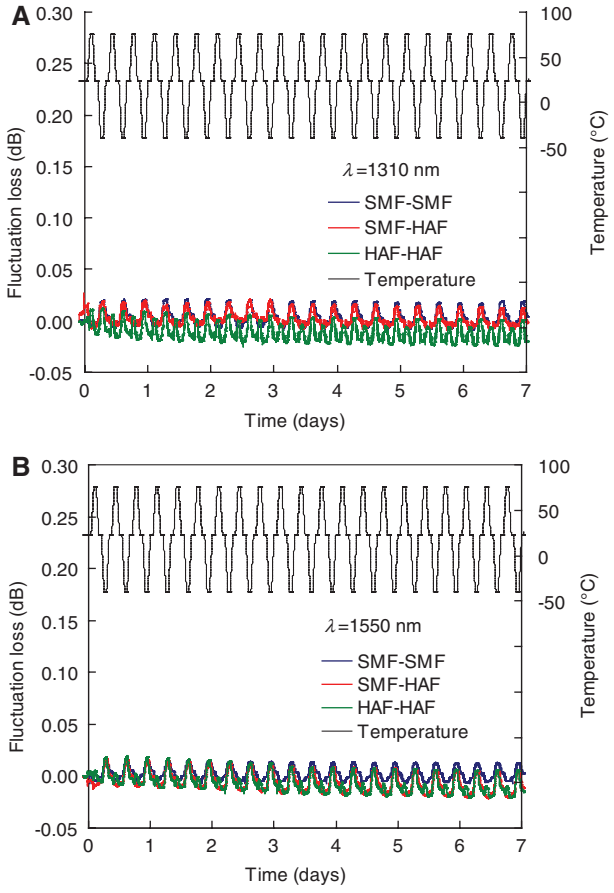


**Figure 17** Temperature cycle test results of mechanical splice (A) at 1310 nm and (B) at 1550 nm.

route in some cases. However, BI-HAF enables network operators to provide optical broadband services in limited space. Moreover, BI-HAF makes it possible to install arbitrary optical in-house wiring, such as tied, returned, and notched wiring, without any special skill.

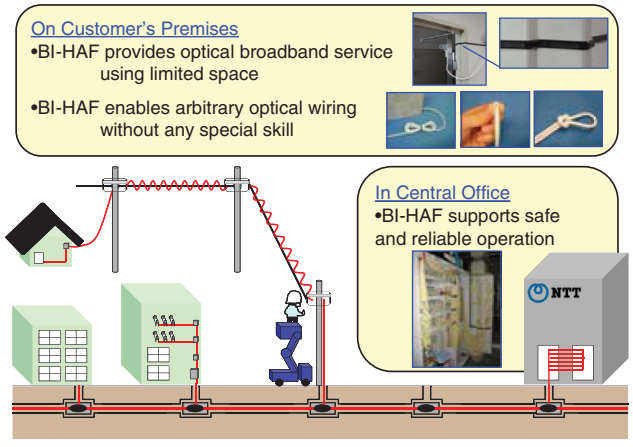


**Figure 18** Schematic image of bending loss insensitive HAF (BI-HAF) applications in optical access network.

A central office can also be considered a BI-HAF application area. As the FTTH network spreads, optical wiring in a central office soon becomes congested. This makes it difficult to conduct easy and safe operation and/or maintenance. Thus, BI-HAF has been utilized to improve the reliability of optical networks. The current applications basically requires a HAF with connectors. It is beneficial to seal the air holes from any contermination. However, the mechanical splice technique enables us to use a HAF without connector, although we need a certain care for storage. As a result, BI-HAF enables us to open up new possibilities for optical networks and to realize reliable and valuable optical networks.

## 5.2 Applicability to high power transmission

The optical power levels used in optical communication networks have been increasing with the development of long unrepeatered submarine systems, dense wavelength-division-multiplexing (DWDM) systems, and distributed Raman amplification systems. Furthermore, the rapid growth in Internet traffic has led to a huge demand for transmission capacity. If we are to meet this exponential demand for capacity, we must greatly increase the optical transmission power. Thus, there is a growing concern about the impact of high optical power on fiber reliability. It has been reported that high optical power can lead to catastrophic damage as a result of the optical fiber fuse phenomenon [33, 34] and failures at bends [35].

A fiber fuse is an optical discharge propagating toward a light source that results in the catastrophic destruction of an optical fiber. Once initiated, the fiber fuse continues to propagate until the light source is shut down or the input power is reduced below the fuse-propagation threshold power. The propagation threshold of a fiber fuse in conventional fiber is as low as 1.2–1.4 W [36]. Therefore, in the near future the fiber fuse phenomenon will pose a real danger to optical communication systems constructed with conventional single-mode fibers [37]. There have already been many experimental and theoretical reports on the fiber fuse phenomenon [20, 33, 34, 36, 38–52]. In addition, several devices have been proposed with a view to avoiding the catastrophic damage caused by a fiber fuse, for example, a fiber fuse terminator using a tapered fiber [53] and a thermally-diffused expanded core (TEC) fiber [54] for an input power of not more than 2 W. A device has been reported that can rapidly detect a fiber fuse and terminate it by monitoring the light backreflected from it [55]. Recently, it was reported that the fuse propagation threshold in HAF [20, 53] can be much higher than

 

that in conventional SMF in the optical communication band.

Here, we first report on the propagation characteristics of a fiber fuse in HAF. We describe how fiber fuse propagation depends on the HAF structure. Then, we report a compact fiber fuse terminator consisting of a short length of HAF. We confirmed the termination of a fiber fuse using a fiber fuse terminator with a 2.5 mm-long HAF when the input power was 21 W.

### 5.2.1 Propagation characteristics of fiber fuse in HAF

The propagation characteristics of the fiber fuse in HAF depend on the relationship between the diameter of an inscribed circle linking the air holes $2R_{In}$ and the diameter of the melted area $D_{melted}$ [20, 51]. The melted area is caused by fiber fuse propagation and $D_{melted}$ is assumed to be almost the same as the size of the optical discharge. When $2R_{In}$ is much larger than $D_{melted}$, the fiber fuse propagates in the same way as in SMF. However, no fiber fuse propagates even at an input power of 18.0 W, when $2R_{In}$ is much smaller than $D_{melted}$ [51, 56].

Figure 19A shows a side view of a splice point between an SMF and HAF-A before and after fiber fuse propagation at a wavelength of 1480 nm. The coupled input power into HAF-A was 8.2 W. HAF-A had six air holes and the core diameter was 9.0 μm. The $2R_{In}$ and hole diameter $d$ of HAF-A were 30.7 and 4.5 μm, respectively. Since $D_{melted}$ was 21 μm at an input power of 8.2 W, $2R_{In}$ was much larger than $D_{melted}$. As shown in Figure 19A, the fiber fuse propagated in HAF-A. The interval between the voids caused by the fiber fuse propagation in HAF-A was 23.6 μm, which is almost the same as that in the SMF. The fuse propagation threshold in HAF-A was 1.3 W at 1480 nm, and was the same as that in a conventional SMF with the same MFD.

In contrast, the fiber fuse terminated near the splice point between SMF and HAF-B, as shown in Figure 19B. The input power coupled into HAF-B was 8.1 W at 1480 nm. HAF-B had six air holes and the core diameter was 9.0 μm. The $2R_{In}$ and $d$ values of HAF-B were 17.1 and 4.6 μm, respectively. Since the $D_{melted}$ in SMF was 21 μm at an input power of 8.1 W, the $2R_{In}$ of HAF-B was smaller than $D_{melted}$. We observed that the air holes in HAF-B were destroyed near the splice point by the fiber fuse, as shown in Figure 19B. No fiber fuse was observed in HAF-B even at an input power of 18.0 W (4.4 W at 1480 nm and 13.6 W at 1550 nm). The fiber fuse did not propagate in HAF-B when we directly heated it with an arc discharge. Therefore, we can consider that the propagation threshold of a fiber fuse in HAF-B is above 18.0 W at around 1550 nm.

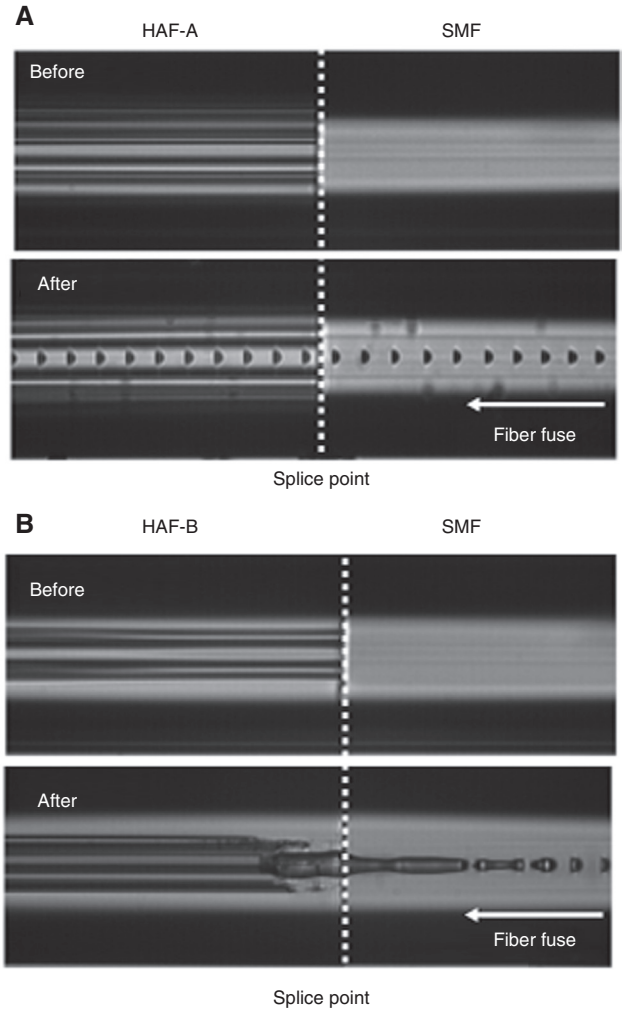


**Figure 19** Side views of a splice point between (A) HAF-A and SMF and (B) HAF-B and SMF before and after fiber fuse propagation at an input power of about 8 W.

This threshold power is more than 10 times that in conventional SMF.

Since the fuse threshold power in conventional SMF is proportional to the MFD [41], we consider that such a high threshold could not be obtained with a method that expands the MFD of conventional SMFs [53, 54].

The mechanism of fiber fuse termination in HAF can be explained as follows [57]. When $D_{melted}$ is larger than $2R_{In}$ as shown in Figure 20A, the optical discharge reaches the air holes. At the same time, a jet of high temperature fluid penetrates the air holes, because the optical discharge is a high temperature fluid under high pressure [34, 48]. That is, the high temperature fluid expands rapidly. This results in a reduction of the temperature and pressure of the optical discharge. Simultaneously, the fiber fuse terminates. An example of the dynamics of fiber fuse termination will be provided in the next section. On the other

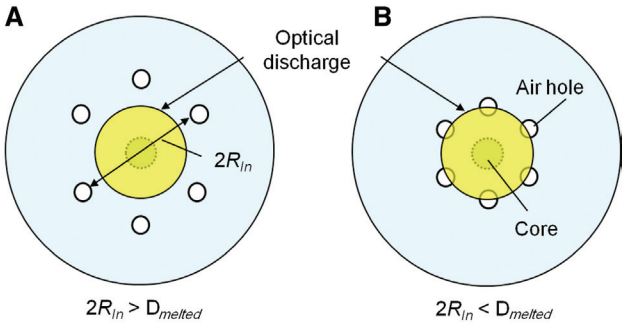


**Figure 20** Relationship between $2R_{In}$ and diameter of optical discharge ($D_{melted}$) in HAF.

hand, the optical discharge does not reach the air holes when $2R_{In}$ is much larger than $D_{melted}$, as shown in Figure 20B. Therefore, no jet of high temperature fluid penetrates the air holes and the fiber fuse does not terminate.

When $2R_{In}$ is almost the same as $D_{melted}$, we observed a new propagation mode with a damage track whose period was approximately 30 times longer than that in conventional SMF [52]. Furthermore, it has been found that the fiber fuse propagation in HAF depends not only on $2R_{In}$ but also on $d$ [57].

### 5.2.2 Compact fiber fuse terminator consisting of HAF

Since the fuse threshold power in HAF can be more than 10 times that in conventional SMF, we proposed a compact fiber fuse terminator consisting of a short length of HAF [58]. Figure 21 shows the structure of our fiber fuse terminator, which consists of a 2.5 mm length of HAF spliced with conventional SMFs. The HAF, which had six air holes, had a core diameter of 9 μm. The $2R_{In}$ and $d$ values of the HAF were 18.6 and 9.1 μm, respectively. The total splice loss between the HAF and SMF was 0.1 dB. Therefore, our fiber fuse terminator is compact and has a simple structure with low loss.

Figure 22 shows the dynamics of the fiber fuse termination near the splice point between the HAF and SMF. The total input power into the HAF was 21 W. The input powers at 1480 and 1550 nm were 8 and 13 W, respectively. These

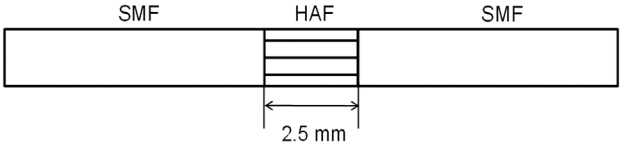


**Figure 21** Structure of fiber fuse terminator.

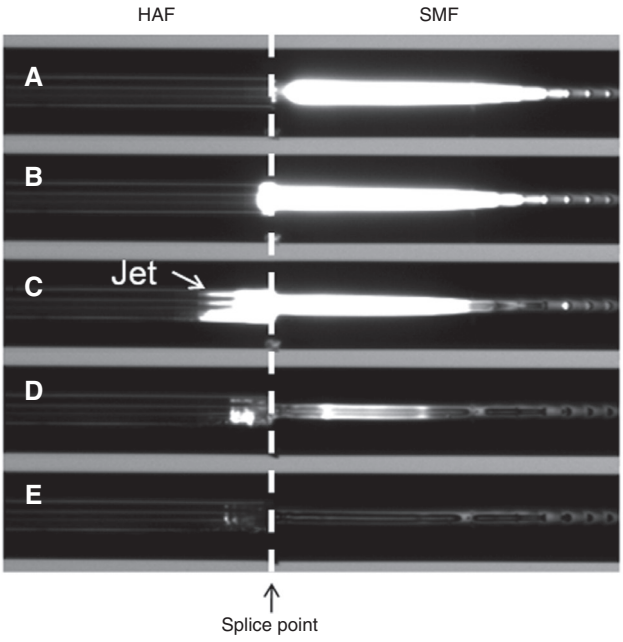


**Figure 22** Dynamics of fiber fuse termination near the splice point between HAF and SMF. The input power was 21 W. The images were obtained at 20 μs intervals.

images were obtained at intervals of 20 μs by using a high-speed camera operating at a speed of $10^5$ fps. As shown in Figure 22 B–D, the front shape of the optical discharge changed at the splice point. Since the optical discharge is considered to be a high temperature fluid under high pressure, its front shape shown in Figure 22C indicates the jet of the high temperature fluid into the air holes. In fact, the diameter of the optical discharge at an input power of 21 W exceeds 23 μm [51], which is much larger than $2R_{In}$ in HAF. Therefore, the high temperature fluid reached the air holes and the jet penetrated the air holes. Then, the optical discharge terminated. The optical discharge penetrated 65 μm into the HAF. Thus we found that we could terminate the fiber fuse propagation by using a fiber fuse terminator consisting of a HAF with a length of only 2.5 mm when the input power was 21 W. It should be noted that in addition to using a fiber fuse terminator, we also need a method for rapidly shutting down the light source when the fiber fuse is initiated. This is because it has been reported that at an input power of over 3 W the optical fiber is heated and burned by the scattered light from the bubble train at the fuse termination point [59].

Above, we reported that the fuse threshold power in HAF can be more than 10 times that in conventional SMF. And we achieved a compact and low-loss fiber fuse terminator composed of a short length of HAF. Furthermore, HAF has a great advantage with a view to avoiding failures at bends under high power [35], because HAF is a

 

low-bending-loss optical fiber [19]. Therefore, we consider HAF to be an attractive optical fiber as a solution for the problems posed by the fiber fuse phenomenon and failures at bends with a high power input [56].

## 6 Conclusion

We reviewed progress on bending loss insensitive hole assisted fiber (BI-HAF) including related technologies. We explained a simple design for HAF that uses an air filling fraction. The transmission properties of BI-HAF were introduced, and the impact of bending loss insensitivity was shown by considering the multi-path interference (MPI) characteristics. These results show that a BI-HAF with the desired properties can be obtained easily by controlling the design conditions of the air holes. The mechanical reliability of the hole assisted structure was also investigated experimentally. Our results showed that there was no noticeable degradation in the mechanical characteristics as a result of introducing air holes. We also described the applicability of various kinds of splicing techniques to BI-HAF. We clarified that BI-HAF can be connected with satisfactory splicing characteristics by appropriately controlling such factors as the endface condition. Some example applications of BI-HAF in access networks were introduced. We showed that BI-HAF enables us to realize the easy and economical construction and/or maintenance of FTTH networks. Finally, we explained the applicability of BI-HAF to high power transmission. We showed that HAF can also be used as a compact fiber fuse terminator. BI-HAF enables us to open up new possibilities for optical networks and realize networks that are both reliable and valuable.

**Acknowledgements:** We thank Mr. Kubozono, Mr. Azuma, Dr. Kurashima, and Dr. Yamamoto for their continuous encouragement.

Received July 7, 2013; accepted September 19, 2013; previously published online October 14, 2013

## References

[1] ITU-T Recommendation G.652. Characteristics of a single-mode optical fibre and cable. 8th ed., Nov. 2009.
[2] Himeno K, Matsuo S, Guan N, Wada A. Low-bending-loss single-mode fibers for fiber-to-the-home. IEEE J Lightwave Technol 2005;23(11):3494–9.
[3] Li MJ, Tandon P, Bookbinder DC, Bickham SR, McDermott MA, Desorcie RB, Nolan DA, Johnson JJ, Lewis KA, Englebert JJ. Ultra-low bending loss single-mode fiber for FTTH. In Proc OFC'08, PDP10, 2008.
[4] Fini JM, Borel PI, Yan MF, Ramachandran S, Yablon AD, Wisk PW, Trevor D, DiGiovanni DJ, Bjerregaard J, Kristensen P, Carlson K, Weimann PA, Martin CJ, McCurdy A. Solid ring-assisted fibers with low bend loss. In Proc OECC'08, ThN2, 2008.
[5] de Montmorillon L-A, Gooijer F, Montaigne N, Geerings S, Boivin D, Provost L, Sillard P. All-solid G.652.D fiber with ultra low bend losses down to 5 mm bend radius. In Proc OFC'09, OTuL3, 2009.
[6] ITU-T Recommendation G.657. Characteristics of a bending-loss insensitive single-mode optical fibre and cable for the access networks, 3rd ed., Oct. 2010.
[7] Kaiser P, Astle HW. Low-loss single-material fibers made from pure fused silica. Bell Sys Tech J 1974;53(6):1021–39.
[8] Okoshi T, Oyamada K. Side-tunnel fibre: an approach to polarisation-maintaining optical waveguiding scheme. IEE Electron Lett 1982;18(19):824–6.
[9] Birks TA, Roberts PJ, Russell P St. J, Atkin DM, Shepherd TJ. Full 2-D photonic bandgaps in silica/sir structures. IEE Electron Lett 1995;31(22):1941–3.
[10] Knight JC, Birks TA, Atkin DM, Russell P. St. J. Pure silica single-mode fibre with hexagonal photonic crystal cladding. In Proc OFC'96, PD3, 1996.
[11] Birks TA, Knight JC, Russell P. St. J. Endlessly single-mode photonic crystal fiber. Opt Lett 1997;22(13):961–3.
[12] Tajima K. Low loss PCF by reduction of hole surface imperfection. In Proc ECOC'07, PD2.1, 2007.
[13] Nakajima K, Zhou J, Tajima K, Kurokawa K, Fukai C, Sankawa I. Ultra wide band 190 Gbit/s WDM transmission over a long length and low loss PCF. In Proc OFC'04, PDP23, 2004.
[14] Kurokawa K, Tajima K, Zhou J, Nakajima K, Matsui T, Sankawa I. Penalty-free dispersion-managed soliton transmission over 100 km low loss PCF. In Proc OFC'05, PDP21, 2005.
[15] Nakajima K, Fukai C, Kurokawa K, Tajima K, Matsui T, Sankawa I. Distributed Raman amplification at 850 nm in a low loss photonic crystal fibre. In Proc ECOC'05, Tu4.4.3, 2005.
[16] Kurokawa K, Tsujikawa K, Tajima K, Nakajima K, Sankawa I. 10 Gb/s WDM transmission at 1064 and 1550 nm over 24 km PCF with negative power penalties. In Proc OECC'07, 12C1–3, 2007.
[17] Ieda K, Kurokawa K, Tajima K, Nakajima K. Visible to infrared high-speed WDM transmission over PCF. IEICE Electron Express 2007;4(12):375–9.
[18] Hasegawa T, Sasaoka E, Onishi M, Nishimura M, Tsuji Y, Koshiba M. Novel hole-assisted lightguide fiber exhibiting anomalous dispersion and low loss below 1 dB/km. In Proc OFC'01, PD5, 2001.
[19] Nakajima K, Hogari K, Zhou J, Tajima K, Sankawa I. Hole-assisted fiber design for small bending and splice losses. IEEE Photon Technol. Lett 2003;15(12):1737–9.
[20] Takenaga K, Tanigawa S, Matsuo S, Fujimaki M, Tsuchiya H. Fiber fuse phenomenon in hole-assisted fibers. In Proc ECOC'08, P.1.14, 2008.
[21] Hanzawa N, Kurokawa K, Tsujikawa K, Matsui T, Tomita S. Suppression of fiber fuse propagation in photonic crystal fiber (PCF) and hole-assisted fiber (HAF). In Proc MOC'09, M7, 2009.

[22] Koshiba M, Hayata K, Suzuki M. Approximate scalar finite-element analysis of anisotropic optical waveguides with off-diagonal elements in a permittivity tensor. IEEE Trans Microwave Theory Tech 1984;MTT-32(6):587–93.
[23] Saitoh K, Koshiba M, Hasegawa T, Sasaoka E. Chromatic dispersion control in photonic crystal fibers: application to ultra-flattened dispersion. Opt. Express 2003;11(8):843–52.
[24] Nakajima K, Shimizu T, Matsui T, Fukai C, Kurashima T. Bending-loss insensitive fiber with hole-assisted structure. IEICE Trans Commun 2011;E94-B(3):718–24.
[25] Ramachandran S, Nicholson JW, Ghalmi S, Yan MF. Measurement of multipath interference in the coherent crosstalk regime. IEEE Photon Technol Lett 2003;15(8):1171–3.
[26] Yu CX, Wang W, Brorson SD. System degradation due to multipath coherent crosstalk in WDM network nodes. IEEE J Lightwave Technol 1998;16(8):1380–6.
[27] ITU-T Recommendation G.650.1. Definitions and test methods for linear, deterministic attributes of single-mode fibre and cable. Amd. 1, Oct. 2010.
[28] Tachikura M, Kurosawa Y, Namekawa Y. Improved theoretical estimation of mechanical reliability of optical fibers. In Proc SPIE 2005;5623:622–9.
[29] Yamada Y, Nakajima K, Kurashima T, Tomita S. Static fatigue characterization with uniform and ultra-small bending. In Proc OFC'11, OMF5, 2011.
[30] Hamada T, Suzuki R, Takenaga K, Guan N, Matsuo S, Himeno K. Arc-fusion splicing techniques for holey fibers. Fujikura Technical Review 2006;35:5–9.
[31] Abe Y, Hoshijima T, Matsui T, Tomita S. Optical characteristics and reliability of mechanical splice utilizing solid refractive index matching material for hole-assisted fiber connection. IEEE Photon. Technol Lett 2009;21(4):194–6.
[32] Saito K, Koyama R, Abe Y, Nakajima K, Kurashima T. Mechanical splice characteristics of hole-assisted fiber. IEEE J Lightwave Technol 2012;30(2):267–72.
[33] Kashyap R, Blow KJ. Observation of catastrophic self-propelled self-focusing in optical fibers. IEE Electron Lett 1988;24:47–9.
[34] Hand DP, Russell P St. J. Solitary thermal shock waves and optical damage in optical fibers: the fiber fuse. Opt Lett 1988;13:767–9.
[35] Percival RM, Sikora ESR, Wyatt R. Catastrophic damage and accelerated aging in bent fibres caused by high optical powers. IEE Electron Lett 2000;36:414–6.
[36] Takenaga K, Omori S, Goto R, Tanigawa S, Matsuo S, Himeno K. Evaluation of high-power endurance of bend-insensitive fibers. In Proc OFC'08, JWA11, 2008.
[37] Morioka T. New generation optical infrastructure technologies: EXAT Initiative towards 2020 and beyond. In Proc OECC'09, FT4, 2009.
[38] Driscoll TJ, Calo JM, Lawandy NM. Explaining the optical fuse. Opt Lett 1991;16:1046–8.
[39] Davis DD, Mettler SC, DiGiovanni DJ. Experimental data on the fiber fuse. In Proc SPIE 1995;2714:202–10.
[40] Atkins RM, Simpkins PG. Track of a fiber fuse: a Rayleigh instability in optical waveguides. Opt Lett 2003;28:974–6.
[41] Nishimura N, Seo K, Shiino M, Yuguchi R. Study of high-power endurance characteristics in optical fiber link. In Proc OAA, TuC4, 2003.
[42] Dianov EM, Bufetov IA, Frolov AA, Chamorovsky YK, Ivanov GA, Vorobjev IL. Fiber fuse effect in microstructured fibers. IEEE Photon Technol Lett 2004;16:180–1.
[43] Shuto Y, Yanagi S, Asakawa S, Kobayashi M, Nagase R. Fiber fuse phenomenon in step-index single-mode optical fibers. J Quantum Electron 2004;40:1113–21.
[44] Dianov EM, Bufetov IA, Frolov AA. Destruction of silica fiber cladding by the fuse effect. Opt Lett 2004;29:1852–4.
[45] Yakovlenko SI. On reasons for strong absorption of light in an optical fibre at high temperature. Quantum Electron 2004;34:787–9.
[46] Dianov EM, Fortov VE, Bufetov IA, Efremov VP, Rakitin AE, Melkumov MA, Kulish MI, Frolov AA. Temperature of optical discharge under action of laser radiation in silica-based fibers. In Proc ECOC'05, We 3.4.4, 2005.
[47] Todoroki S. Origin of periodic void formation during fiber fuse. Opt Express 2005;13:6381–9.
[48] Yakovlenko SI. Mechanism for the void formation in the bright spot of a fiber fuse. Laser Physics 2006;16:474–6.
[49] Akhmediev N, Russell P. St. J, Taki M, Soto-Crespo JM. Heat dissipative solitons in optical fibers. Physics Lett A 2008;372:1531–4.
[50] Takara H, Masuda H, Kanbara H, Abe Y, Miyamoto Y, Nagase R, Morioka T, Matsuoka S, Shimizu M, Hagimoto K. Evaluation of fiber fuse characteristics of hole-assisted fiber for high power optical transmission systems. In Proc ECOC'09, P.1.12, 2009.
[51] Hanzawa N, Kurokawa K, Tsujikawa K, Matsui T, Nakajima K, Tomita S, Tsubokawa M. Suppression of fiber fuse propagation in hole assisted fiber and photonic crystal fiber. J Lightwave Technol 2010;28:2115–20.
[52] Hanzawa N, Kurokawa K, Tsujikawa K, Takenaga K, Tanigawa S, Matsuo S, Tomita S. Observation of a propagation mode of a fiber fuse with a long-period damage track in hole-assisted fiber. Opt Lett 2010;35:2004–6.
[53] Hand DP, Birks TA. Single-mode tapers as 'fiber fuse' damage circuit-breakers. Electron Lett 1989;25:33–4.
[54] Yanagi S, Asakawa S, Kobayashi M, Shuto Y, Nagase R. Fiber fuse terminator. In Proc LEOS'03 2003;1:386.
[55] Abedin KS, Nakazawa M, Miyazaki T. Backreflected radiation due to a propagating fiber fuse. Opt Express 2009;17: 6525–31.
[56] Kurokawa K. Optical fiber for high-power optical communication. Crystals 2012;2:1382–92.
[57] Kurokawa K, Hanzawa N, Tsujikawa K, Tomita S. Hole-size dependence of fiber fuse propagation in hole-assisted fiber (HAF). In Proc MOC'11, H-30, 2011.
[58] Kurokawa K, Hanzawa N. Fiber fuse terminator for above 20 W input. In Proc SSDM'12, A-3-3 2012:546–7.
[59] Yamada M, Koyama O, Katsuyama Y, Shibuya T. Heating and burning of optical fiber by light scattered from bubble train formed by optical fiber fuse. In Proc OFC'11, JThA1, 2011.